THE JOURNAL OF PHYSICAL CHEMISTRY C
A JOURNAL OF THE AMERICAN CHEMICAL SOCIETY

pubs.acs.org/JPCC

Article

Molecular Capacitor Discharge as a Probe of Film Restructuring at Low Temperatures

Roey Sagi, Michelle S. Akerman, Carmen Tamburu, and Micha Asscher*

Cite This: J. Phys. Chem. C 2024, 128, 651−657

Read Online

ACCESS | Metrics & More | Article Recommendations | Supporting Information

ABSTRACT: Discharge of weakly bound, positive, and negative charges upon annealing of atomic and molecular layers that form a nanocapacitor is demonstrated as a sensitive detection method of low-temperature restructuring of films, such as densification, phase transitions, and desorption. This is detected by employing temperature-programmed contact potential difference (TP-ΔCPD) measurements utilizing a Kelvin probe within an ultrahigh-vacuum environment. Onset temperature for the discharge and its profiles are shown to be dependent on the film growth temperature but independent of the charge identity. The discharge is triggered by the restructuring processes, as demonstrated for very different materials—Kr, CD_3Cl, and amorphous solid water (ASW) films. The discharge phenomenon leads to a deeper and better understanding of the complex low-temperature processes that take place within molecular films, often at temperatures significantly lower than their onset for desorption.

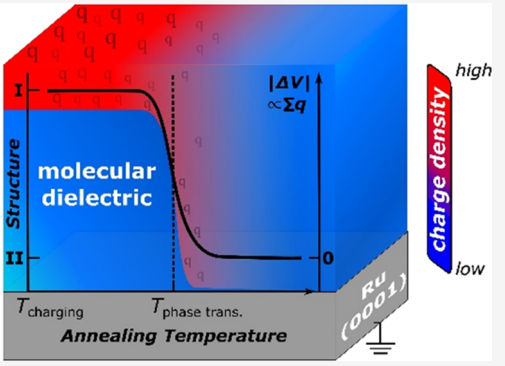

1. INTRODUCTION

Temperature-programmed contact potential difference (TP-ΔCPD) measurements and their derivative, d(ΔCPD)/dT, typically recorded via an in vacuum Kelvin probe, are complementary methods to temperature-programmed desorption (ΔP-TPD). While ΔP-TPD monitors adsorbates upon their removal to the gas phase, TP-ΔCPD provides information on atoms/molecules that are in their adsorbed state.[1] Thus, in the absence of other competing processes, the d(ΔCPD)/dT spectrum recorded for thin films is directly proportional to the desorption rate obtained during ΔP-TPD measurements. An advantage the TP-ΔCPD method has over ΔP-TPD (also for thick films) is its capability to sense dynamic processes that the adsorbed film undergoes at temperatures significantly lower than the onset for desorption.

TP-ΔCPD measurements were shown to be beneficial in the study of dielectric properties of thick molecular films (ices), with focus on crystalline and amorphous solid water (ASW), either neutral or charged.[2−10] In the latter case, the possible effect of the nature of the charging (positive or negative) has not been addressed so far.

Following adsorption of thick layers, the ΔCPD is expressed as the difference $\Delta CPD_{substrate/film\ interface} - V_{film}$, where V_{film} is the potential that may spontaneously evolve within the adsorbed film between its interfaces with the substrate and the surrounding medium (herein, the vacuum). If $|V_{film}| > 0$ and independent of film temperature, then the polarization of the film will be modified only due to the removal of adsorbed layers while TP-ΔCPD will still be comparable and proportional to ΔP-TPD. This, however, is rarely the case, as V_{film} of thick molecular films grown at low temperatures often exhibits a strong dependence on temperature.[11−14] Moreover, spontaneous polarization that may be developed within molecular films, also termed as spontelectric effect, often depends on the porous nature of films when grown at low temperatures.[6,12,13]

Once a molecular film is bombarded by low-energy charges (electrons or positive ions, at a low enough energy to avoid removal or dissociation of molecules within the film), these charges accumulate near its vacuum interface.[4,15,16] The charged film, if stable enough at the interface, typically obeys a classical plate capacitor physics.[2,4,5,8,16] Here, the charged interface with the vacuum forms the "top" electrode, whereas the interface with the metallic substrate forms the "bottom" one. The potential difference evolving between the two "plates", ΔV, can be expressed as

$$\Delta V = V_{film}^{charged} - V_{film}^{neutral} = \frac{QL}{A\varepsilon_0\varepsilon_{(T)}} \quad (1)$$

where Q indicates accumulated charges, A is the area exposed to the impinging charges (taken as the area of the substrate), L is the distance between the plates (approximately the film thickness), ε_0 is the vacuum permittivity, and $\varepsilon_{(T)}$ is the temperature-dependent relative permittivity of the film. These nanocapacitors were demonstrated to develop extremely high

Received: November 17, 2023
Revised: November 30, 2023
Accepted: December 4, 2023
Published: December 20, 2023

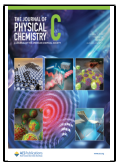

https://doi.org/10.1021/acs.jpcc.3c07591
J. Phys. Chem. C 2024, 128, 651−657

electric fields, more than 10^8 V/m.[4,5,17] Such fields may affect the orientation of guest molecules embedded within the host ice[17] and potentially (at even higher fields) can catalyze their reactivity.[18] Charging of molecular films by low-energy electrons and ions is a fundamental process that occurs throughout the universe. It results from the interaction of condensed matter with high-energy radiation, e.g., cosmic rays, γ-rays, X-rays, UV light, ion beams, and free electrons, with implications on diverse fields,[19] including environmental and life sciences,[20] medicine,[21−23] as well as astrochemistry.[24,25]

2. METHODS

The current experiments were performed in an ultrahigh-vacuum environment (UHV; base pressure of 2×10^{-10} Torr), where an 8×8 mm^2 Ru(0001) substrate is held at the center of the UHV chamber, attached to a closed-cycle He refrigerator. The substrate is cleaned daily by 15 min of sputtering using 1000 eV Ne^+ ions, followed by 10 min annealing at 1450 K. Films were grown on top of the substrate by backfilling the UHV chamber with the designated gaseous species. Bombardment of the films either with low-energy electrons (3 eV; emitted from a Kimball Physics, ELG-2 electron gun) for 60 s or with low-energy Ne^+ ions (85 eV; generated by a Varian, 981−2043 sputter-gun;) for 10 s leads to their respective negative or positive charging. The electron energy is sufficiently far from the minimum energy for dissociative electron attachment (DEA),[26,27] and the Ne^+ ion energy does not sputter the films. Charging parameters are held identical to those generating through-the-bare substrate transmission currents, I_0, of 1.0 μA and 10 nA for electrons and Ne^+ ions, respectively. Once charging is completed, the substrate is heated at a rate of 1 K/s while a Kelvin probe (Au-plated mesh, 2 mm in diameter wide; Besocke Delta-PHI, type S) monitors the contact potential difference (CPD; measurements are typically referenced to the state of the clean substrate and thus referred to as ΔCPD). Then, a smoothing procedure of the ΔCPD signal recorded upon heating enables to obtain its numerical derivative with respect to temperature, namely, the d(ΔCPD)/dT spectra. Desorption of molecules from the substrate or from the films is (separately) monitored by a quadrupole mass spectrometer (SRS, RGA 200) via ΔP-TPD measurements. Further details on the experimental setup can be found in the Supporting Information.

In this report, we demonstrate that a correlation found between d(ΔCPD)/dT and ΔP-TPD spectra is not limited to specific thin films; it is a rather general phenomenon and applies for atomic/molecular films with significantly different nature of interactions among the atoms and molecules that form the films. This is shown here for Kr, H_2O, and CD_3Cl films. The main results of this work have been that the drop in the measured voltage across charged films upon heating is interpreted as a discharge (of both positive and negative charges), triggered by structural changes within the molecular films.

3. RESULTS AND DISCUSSION

3.1. Charging of Kr Films. In Figure 1, a comparison is presented between d(ΔCPD)/dT and ΔP-TPD spectra for nonpolar (V_{film} = 0), 500-monolayers (ML)-thick Kr atoms films grown on top of a Ru(0001) substrate at a growth temperature (T_{gr}) of 33 K. Because V_{film} = 0, the d(ΔCPD)/dT spectrum of thick neutral Kr film (black solid line) is sensitive only to the desorption of the bottom-most monolayer (Kr ΔP-TPD spectra of 1 and 500 ML are shown in orange dashed and solid lines, respectively). However, modification of the surface polarization by charging the film enables the Kelvin probe to monitor the multilayer desorption as well; see the blue (positive charging) and red (negative charging) differential d(ΔCPD)/dT profiles in Figure 1.

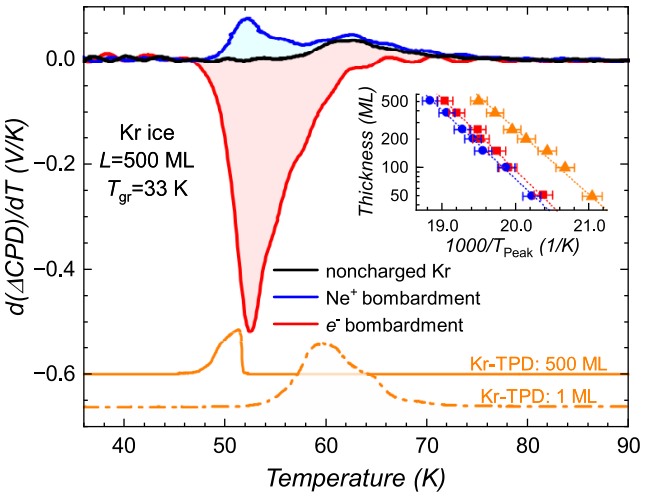

Figure 1. Desorption of nonpolar Kr films, as detected by a Kelvin probe. d(ΔCPD)/dT spectra of neutral, 500-ML-thick Kr ice grown at 33 K (black solid line) and of charged Kr films (red and blue lines) are demonstrated. Charged films were formed by their bombardment with low-energy charges, either negative (3.0 eV electrons, red) or positive (85 eV Ne^+, in blue). Solid and dashed orange lines are the ΔP-TPD spectra of 500- and 1-ML-thick Kr films, respectively (not to scale). Inset: Film thickness (ML) vs the reciprocal of the (shifted to higher temperature with thickness) multilayer desorption peak temperature (T_{peak}), as obtained from ΔP-TPD measurements (orange triangles) and from the d(ΔCPD)/dT spectra of the Kr films, either negatively (red squares) or positively (blue circles) charged.

Charging the Kr film by low-energy electrons or Ne^+ ions polarizes the film. In the case of positive charging, Ne^+ ionizes Kr atoms at the top of the Kr film to form a layer of Kr^+ (transforming the film into an effective plate capacitor). The Ne^+ ions are subsequently scattered back to the gas phase as neutral Ne atoms, as previously shown for ASW films employing Ar^+ or Ne^+ ions.[4,10] The charge transfer (from Kr to Ne^+) occurs due to the higher ionization energy of Ne relative to that of the Kr atoms within the atomic ice, 21.6 and 11.9 eV, respectively.[28,29] Voltage drop (discharge) of the charged Kr ice upon subsequent annealing is displayed in Figure 1 by the red and blue lines following negative and positive charging, respectively. The blue and red filled areas, below and above the spectrum of the noncharged ice (black solid line), mark the potential difference between the two "electrodes" of the nanocapacitor (ΔV) for each type of charging. We note that the differential profiles [d(ΔCPD)/dT] of both the positive and the negative charging extend beyond the multilayer desorption peak (at temperatures above 52 K). It can be explained only if some of the charged Kr ions are stabilized by Kr atoms surrounding them at monolayer coverage or that 3D islands that include residual charging are stabilized at temperatures above 52 K. This issue, however, requires further investigation.

https://doi.org/10.1021/acs.jpcc.3c07591
J. Phys. Chem. C 2024, 128, 651−657

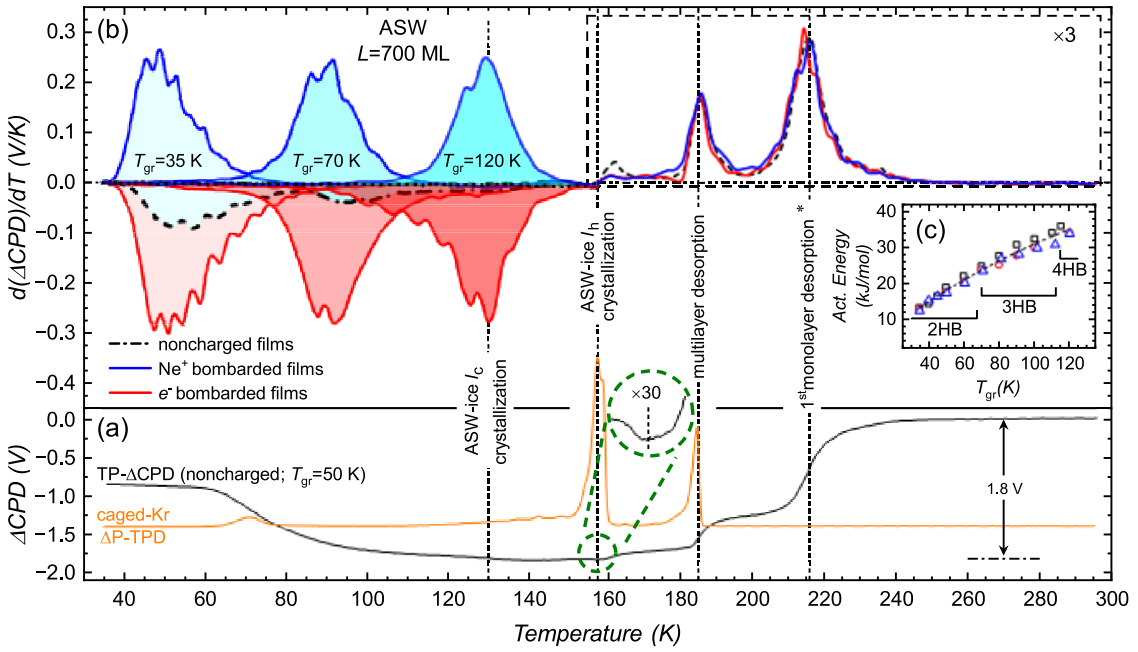

Figure 2. Restructuring and phase transitions of ASW as detected by a Kelvin probe. (a) TP-ΔCPD profile (black solid line) of a noncharged 700-ML-thick ASW film grown at 50 K. (b) d(ΔCPD)/dT spectra of noncharged (black dashed lines), negatively charged (red) and positively charged (blue) ASW films. Layers were grown at the indicated growth temperatures (T_{gr}) and were subsequently charged either positively or negatively, both at a fixed charging temperature of 35 K. The d(ΔCPD)/dT spectra are compared to ΔP-TPD measurements of caged Kr atoms co-deposited within a noncharged ASW film grown at 35 K [orange solid line in (a); Kr dose is equivalent to 1 ML]. (c) Dependence on the growth temperature of the apparent activation energy for depolarization and for the binding energies of the charges (in matching colors). Dominant number of hydrogen bonds per water molecule is indicated as 2HB, 3HB, and 4HB for 2, 3, and 4 hydrogen bonds, respectively, based on IR measurements and interpretation in the literature.[6]

Thickness-dependent TP-ΔCPD study of Kr films (see inset of Figure 1) reveals the typical zero-order kinetics of multilayer film desorption. The zero-order kinetics is demonstrated by a shift of the d(ΔCPD)/dT peak to a higher temperature as the film thickness increases (red squares and blue circles for negative and positive charging, respectively). The temperature of the multilayer desorption peak is valuable for extracting the apparent energetics of the interatomic interaction. This can be obtained since the film thickness is proportional to $\int_{T_0}^{T_{peak}} \exp(-E_{des}/k_B T)dT$, where E_{des} is the activation energy for desorption, k_B is the Boltzmann constant, T_0 is the onset temperature for the multilayer desorption, and T_{peak} is the multilayer desorption peak temperature (Redhead analysis).[30] Due to the small changes in T_{peak} as the film thickness increases (of only a few degrees), the result of the integral can be approximated to $A_0 \exp(-E_{des}/k_B T_{peak})$. Fitting the data to this Arrhenius-like expression yields an apparent activation energy for the desorption of Kr atoms from its multilayer of 14 ± 2 kJ/mol, in agreement with the 13 ± 2 kJ/mol value extracted from equivalent ΔP-TPD measurements of noncharged films (orange triangles) and slightly above the sublimation energy of Kr atoms of 11 kJ/mol, as reported in the literature.[31] The smaller area under the positive charging (blue in Figure 1), compared to the negative charging (in red), is attributed to a lower level of the initial charging, as a result of the very different flux and energy. Although the charging level is lower, the efficiency of the positive charging exceeds that of the negative one. In both cases, the charging is very stable for a long duration (see Figure S1 in the Supporting Information).

3.2. Charging of ASW Films. Thick water layers grow as amorphous solid (ASW)[32] and are porous at adsorption temperatures below 115 K.[33] This is attributed primarily to their permanent dipole moment and the hydrogen bonding that they form among neighboring water molecules. Investigations have shown that ASW films develop spontaneous polarization, with the present-day understanding that their porous structure governs the polarization of the films and its voltage buildup.[6,12,34] Molecules on pore walls (partially) orient their dipoles with a component in the direction normal to the substrate plane. These dipoles accumulate during film growth and eventually form a significant degree of macroscopic polarization within the film. An irreversible depolarization is recorded when the films are annealed.[12] During the annealing process, the porous structure collapses and leads to densification and depolarization of the film.[6,35,36]

The morphology of ASW films is significantly affected by the growth conditions, where the porosity and density of the ASW films are primarily dictated by the growth temperature. The porosity of ASW decreases as the substrate temperature at film growth (T_{gr}) increases,[37,38] turning into a compact film (nonporous) at T_{gr} above 115 K. TP-ΔCPD measurements of ASW films show only minor changes in polarization at annealing temperatures below their respective T_{gr}. In contrast, at annealing temperatures above T_{gr}, a significant change in the film polarization is detected. This is demonstrated in Figure 2a for a 700-ML-thick ASW film grown at 50 K and then cooled to 35 K prior to its annealing (black solid line). TP-ΔCPD measurements comparing charged and noncharged films of ASW clearly demonstrate this point, as demonstrated in Figure S2 in the Supporting Information. The d(ΔCPD)/dT spectra of noncharged films grown at T_{gr} in the range 35−120 K and then cooled down to 35 K (black dashed lines in Figure 2b) reveal that the broad low-temperature depolarization peak

https://doi.org/10.1021/acs.jpcc.3c07591
J. Phys. Chem. C 2024, 128, 651−657

shifts to higher temperatures, coupled to the increase in T_{gr}. A comparison between TP-ΔCPD measurements and temperature-dependent infrared absorbance around 3700 cm^{-1} assigned to undercoordinated water dangling bonds demonstrates a nice overlap in terms of their thermal response and spectral breadth.[6] Eventually, the growth temperature imposes a unique morphology, as reflected by a specific polarization change upon heating. Regardless of a particular T_{gr} value, there is an annealing temperature (130 K), above which all of the spectra overlap,[12] reflecting an identical structure prior to desorption of the water film (multilayer desorption onset at 140 K). A Redhead-like analysis[30] of the depolarization peak is used to extract apparent activation energies for depolarization in the range of 12.5−39.0 kJ/mol (black squares in Figure 2c).

Once adsorbed on cold surfaces, water molecules may trap coadsorbed atoms and molecules[38] and can compress and cage preadsorbed ones[39−41] due to their strong interaction with substrates and among themselves (via hydrogen bonding). Upon annealing, the caged (weakly interacting) guest molecules explosively desorb at the onset and during the crystallization process of the host ASW film at a characteristic desorption peak width of 2−3 degrees. A second desorption peak of the guest molecules follows the multilayer desorption of the host molecules at higher temperature. The explosive desorption is termed the *"molecular volcano"*[41] and was demonstrated for various weakly interacting species trapped inside ASW films.[42] Recently, the reversed process of abrupt ejection toward the substrate has been demonstrated for guest molecules that strongly interact with the substrate (NH_3@ASW), coined *"inverse-volcano"*.[43]

Co-depositing ASW films with small quantities of inert atoms, e.g., Kr, has been demonstrated to be useful for monitoring structural changes occurring within the host matrix at temperatures below crystallization, due to the formation of cracks which provide escape routes of the caged species to the gas phase.[38,42]

The d(ΔCPD)/dT spectra may then be compared with a ΔP-TPD measurement of co-deposited Kr within ASW film, grown at 35 K, here at a total Kr dose of 1 ML. The comparison reveals that polarization changes within the host molecular matrix occur at the same temperatures that are indicated by the desorption of the Kr atoms (orange line in Figure 2a at 157 K and 185 K). In other words, both phenomena originate from the same macroscopic events the films undergo. These are assigned to crystallization to the hexagonal ice (ice I_h) at 157 K, leading to the "atomic volcano", and at the high-temperature peak to the multilayer desorption of the host ASW matrix (at 185 K for 700-ML-thick film, 1 K/s heating rate). A small fraction of the Kr atoms desorb at lower temperatures (∼70 K), apparently from the film−vacuum interface, signifying the weak interaction of Kr atoms with water molecules.

Following charging, annealing of the ASW films leads to a sensitive probe of the restructure of the films via the voltage drop observed in the TP-ΔCPD spectrum, as demonstrated in Figure 2a by the solid black line. In addition, the red and blue lines of the differential spectra [d(ΔCPD)/dT] for negatively (red) and positively (blue) charged films follow the same temperature dependence, as shown in Figure 2b. The most striking observation is that the discharge profiles are independent of charge sign, resulting in a mirror-image-like behavior. Moreover, the highest discharge rate, as measured during TP-ΔCPD measurements, is obtained exactly at the same temperature as the highest depolarization rate measured in neutral films grown at the same T_{gr}. Overall, neutral and charged films display almost identical TP-ΔCPD profiles (see Figure S2 in the Supporting Information); however, as expected, the charged ices present much more intense d(ΔCPD)/dT signals. The independence of the discharge profiles on the charge type is a surprising observation that has not been demonstrated before, and is not yet a well-understood behavior because of the different nature of interaction of the two opposite charges. A Redhead-like analysis is employed for extracting apparent binding energies of both the positive and negative charges (red circles and blue triangles in Figure 2c). These apparent binding energies can be correlated with the populations of dangling bonds, known to be affected by and modified during heating of the films, and to the nature of the charge binding sites. From a comparison to the work of Bu et al.,[6] we conclude that depolarization and discharge upon annealing of ASW films grown at T_{gr} below 70 K occur at the same temperature and therefore are proposed to be correlated with a decay of the integrated IR absorbance at 3720 cm^{-1}, which has been assigned to two-coordinated water molecules (denoted as 2HB in Figure 2c). At this T_{gr} range, the intensity of three-coordinated water molecules (IR absorbance near 3696 cm^{-1}; denoted as 3HB in Figure 2c) barely changes. From their data, films that are grown at 70 K should not show any IR peak near 3720 cm^{-1}.[6] At T_{gr} above 70 K, the integrated intensity of the IR band at 3696 cm^{-1} for the three-coordinated water molecules decays as well, and at 120 K, this peak vanishes,[6] signifying the dominance of a fully compact film where each water molecule possesses four hydrogen bonds (4HB in Figure 2c). This configuration results in the formation of higher stability sites for trapped charges. Moreover, the increasing binding energies of both negative and positive charges with the number of hydrogen bonds per (water) molecule at exactly the same pattern are a new observation. The fact that the discharge profiles follow the depolarization of the neutral films suggests that the discharge occurs *in response to* structural modifications within the film, such as pore collapse in the case of films grown at low T_{gr}.

We conclude, therefore, that the charging with subsequent discharge of such films does not induce the structural modification but rather amplify the ΔCPD signature of these identical structural changes. A comparison of the amplitude of the discharge profile via the d(ΔCPD)/dT signal to that of the thermal ΔCPD response of neutral films shows that it is amplified by a factor of 3 at T_{gr} = 35 K and by a factor of 6 at T_{gr} = 70 K. The amplification factor depends on the extent of charging.

The d(ΔCPD)/dT spectra of noncharged ASW films grown at T_{gr} < 120 K reveal a minor change in polarization around 130 K.[12] When discussing films grown at T_{gr} = 120 K, this change can barely be seen, as it is reduced to the limit of the detectability of the probe. In contrast, ASW films grown at 120 K and subsequently charged reveal a sharp peak at 130 K upon annealing. This peak intensity is enhanced by a factor of 75 relative to the intensity recorded for noncharged films when grown at low temperatures. This peak is tentatively assigned to the amorphous-to-cubic ice (ice I_c) phase transition.[32,44] Assuming this assignment is correct, the fact that no measurable Kr atomic volcano is associated with it at 130 K, in contrast to the phase transition to the ice I_h crystalline phase at 157 K (see Figure 2a) suggests that only a small fraction of the ASW crystalizes to the cubic phase. Above 115 K, the films

https://doi.org/10.1021/acs.jpcc.3c07591
J. Phys. Chem. C 2024, 128, 651−657

are expected to be compact and thus should not be polar anymore (unlike the case of the low-temperature growth). Since the neutral films are nonpolar, changes in the relative permittivity cannot affect our Kelvin probe measurement. The fact that the voltage drop (discharge) dramatically enhances this feature leads us to propose that *discharge* follows this macroscopic molecular movement (phase transition) rather than a dielectric response. The differential discharge [via the d(ΔCPD)/dT spectra] is wide and structured and therefore should reflect energetically different binding sites that appear very similar for both negative and positive charges.

3.3. Charging of CD_3Cl Films. The discussion above has so far demonstrated the effect of charging on inert atoms (Kr) and the well-studied system of ASW. Recent studies have shown that various polar organic molecules spontaneously form highly polar films upon their condensation under UHV conditions at cryogenic temperatures.[7,9,11] Subsequent annealing results in nonreversible depolarization profiles that are remarkably similar to the TP-ΔCPD profiles presented here. In order to explore to what extent the charging effects are general among different molecular films, we have extended our study to the behavior of nonpolar molecular films (V_{film} = 0) composed of dipolar molecules that do not form hydrogen bonding. This is the case of the methyl chloride (CD_3Cl) films. The macroscopic minimal level of polarity of the film during growth is apparently due to the antiparallel nature of consecutive layers in the film.[39]

Methyl chloride does not form a significantly polar film upon its growth. This is indicated by ΔCPD measurements conducted during the adsorption of thick molecular CD_3Cl films, as demonstrated in Figure S3 in the Supporting Information. Nevertheless, TP-ΔCPD measurements (Figure 3a) can still record a macroscopic motion of the molecular dipoles during film restructure, as demonstrated in the 10-fold magnified d(ΔCPD)/dT spectra of neutral films (black dashed lines in Figure 3b). Comparison of ΔP-TPD spectrum of co-deposited Kr atoms with methyl chloride films (orange line) and d(ΔCPD)/dT spectra of neutral and charged methyl chloride films reveals that crystallization apparently occurs at 71 K, as detected via the "volcano" desorption of the Kr atoms at this temperature. Methyl chloride in-vacuum crystallization has not been reported so far in the literature, as far as we know. The d(ΔCPD)/dT spectra in Figure 3b suggest that the films of methyl chloride are nonporous. Evidence for the apparent compact morphology of this molecular film is indicated by the absence of a peak at temperatures below that of crystallization. As in the ASW films, charging with subsequent discharge significantly amplifies (here by a factor of 60) peaks observed in the noncharged d(ΔCPD)/dT spectra, regardless of positive or negative charges.

The smaller amplitude of the positive derivative signal (blue area in Figure 3b) may arise from a less stable positive charging of the "molecular capacitor" of CD_3Cl when compared with the negative charging (the red area in Figure 3b). However, as demonstrated in Figure S1 in the Supporting Information, in both cases, only a minor voltage drop appears, indicating the formation of a stable "top plate". One must also consider the 2 orders of magnitude lower dosage of Ne^+ ions colliding with the films.

Ionization of the films by the impinging Ne^+ ions at the film−vacuum interface, and as a result, the positively charged layer formation is more efficient than the direct electrons charging, stabilization, and negatively charged layer formation.

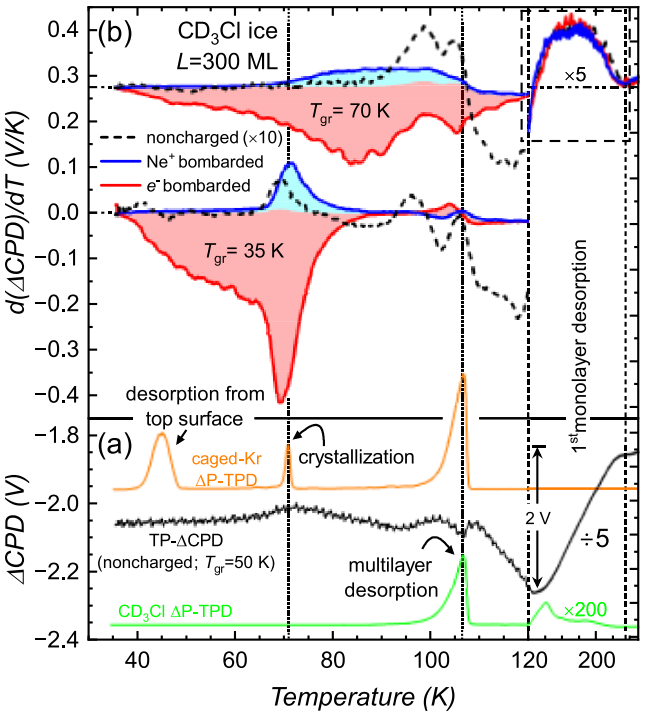

Figure 3. Restructuring and phase transitions of solid methyl chloride (CD_3Cl) films. (a) TP-ΔCPD profile (black solid lines) of a noncharged 300-ML-thick CD_3Cl film grown at 50 K. In addition, ΔP-TPD spectra of pure 300-ML-thick CD_3Cl film, in green, and of Kr atoms co-deposited with 300-ML-thick CD_3Cl film (total Kr dose of 1 ML), in orange, are presented. (b) d(ΔCPD)/dT spectra of noncharged and charged 300-ML-thick CD_3Cl films grown at either 35 or 70 K (and then cooled down to 35 K before recording the spectrum), as indicated. The d(ΔCPD)/dT spectra of the noncharged films (dashed black lines) are magnified 10-fold. Vertical positions of the ΔP-TPD and d(ΔCPD)/dT spectra are arbitrarily shifted on the y-axis for clarity.

This is manifested by the 2 orders of magnitude higher current necessary for charging the films with electrons. This observation results also in a thicker negatively charged "top plate" (exact number of charged layers cannot exactly determined) when compared with the positive ionization process. This, however, should not affect the "plate capacitor" physics we consider because of the large thickness of the entire films we study.

4. CONCLUSIONS

The present study demonstrates that TP-ΔCPD spectra and their associated differential mode of d(ΔCPD)/dT can monitor high coverage molecular desorption, similar to ΔP-TPD, enabling the extraction of binding energies of positive and negative charges to the host molecular films, as shown for Kr, CD_3Cl, and ASW. In addition, it provides information on the kinetics of various restructure processes, such as densification and phase transition within the investigated films as temperature increases. It is shown that the type of charging (negative or positive) does not affect the temperature at which discharge takes place. This is due to the main observation of this study, namely, that structural changes within atomic and molecular films, having very different thermal and chemical properties, are the driving force for the discharge events of the positively and negatively charged films.

https://doi.org/10.1021/acs.jpcc.3c07591
J. Phys. Chem. C 2024, 128, 651−657

This is indicated by Kelvin probe measurements in the case of *noncharged films*.

This conclusion is in contrast to earlier studies by Cowin and co-workers,[45] who claimed that the observed voltage drop (or rise) during temperature increase of charged films (revealed through the TP-ΔCPD spectra) occurs exclusively due to very large, compensating, temperature effects on the relative permittivity (dielectric constant, $\varepsilon_{(T)}$) of such films. This study was limited only to positive charging of the ASW film (by D_2O^+ and Cs^+). This hypothesis, however, without a direct, *in situ, in vacuum* way to detect or measure the changing value of $\varepsilon_{(T)}$ and the fact that both the positive and negative charges should then keep residing on the top film−vacuum interface even after the voltage change has taken place at a higher temperature is physically unlikely to explain the entire picture. Nevertheless, one cannot exclude the possibility that our view of discharge at the restructure temperature takes place together with some (unknown) modification in the relative permittivity of the film as well. The thermal behavior of molecular films and their structural changes, magnified when these films are charged when monitored by a Kelvin probe, provides an insight into the stability and failure issues of nonconducting solids in general.

■ ASSOCIATED CONTENT

Supporting Information

The Supporting Information is available free of charge at https://pubs.acs.org/doi/10.1021/acs.jpcc.3c07591.

Detailed description of the experimental setup, methods, and materials used in this study; charging stability with time of charged Kr and CD_3Cl films as well as ΔCPD monitoring during growth of a CD_3Cl film; and comparison between charged and noncharged ASW and CD_3Cl films (PDF)

■ AUTHOR INFORMATION

Corresponding Author

Micha Asscher − *Institute of Chemistry, Edmond J. Safra Campus, Givat-Ram, The Hebrew University of Jerusalem, Jerusalem 9190401, Israel;* orcid.org/0000-0002-4476-5617; Email: micha.asscher@mail.huji.ac.il

Authors

Roey Sagi − *Institute of Chemistry, Edmond J. Safra Campus, Givat-Ram, The Hebrew University of Jerusalem, Jerusalem 9190401, Israel;* orcid.org/0000-0001-8872-0683

Michelle S. Akerman − *Institute of Chemistry, Edmond J. Safra Campus, Givat-Ram, The Hebrew University of Jerusalem, Jerusalem 9190401, Israel;* orcid.org/0000-0001-8652-7513

Carmen Tamburu − *Institute of Chemistry, Edmond J. Safra Campus, Givat-Ram, The Hebrew University of Jerusalem, Jerusalem 9190401, Israel*

Complete contact information is available at: https://pubs.acs.org/10.1021/acs.jpcc.3c07591

Author Contributions

R.S. designed and performed all of the experiments, analyzed the data, and wrote the manuscript. M.S.A. performed part of the positive charging experiments of the ASW films and contributed to the data analysis. C.T. assisted in parts of the experimental effort. M.A. is responsible for the entire study and wrote the manuscript together with R.S.

Notes

The authors declare no competing financial interest.

■ ACKNOWLEDGMENTS

Partial support by the Israel Science Foundation (ISF, Grant Number 1406/21) and by the Einstein Foundation, Berlin, is acknowledged. Technical support provided by Dr. Eduard Mastov, Marcelo Friedman, Shaul Binyamini, Alexander Lantsman, and the staff of the Racah Institute of Physics workshop is greatly appreciated.

■ REFERENCES

(1) Pfnür, H.; Feulner, P.; Menzel, D. The Influence of Adsorbate Interactions on Kinetics and Equilibrium for CO on Ru(001). II. Desorption Kinetics and Equilibrium. *J. Chem. Phys.* **1983**, *79* (9), 4613−4623.

(2) Iedema, M. J.; Dresser, M. J.; Doering, D. L.; Rowland, J. B.; Hess, W. P.; Tsekouras, A. A.; Cowin, J. P. Ferroelectricity in Water Ice. *J. Phys. Chem. B* **1998**, *102* (46), 9203−9214.

(3) Tsekouras, A. A.; Iedema, M. J.; Ellison, G. B.; Cowin, J. P. Soft-Landed Ions: A Route to Ionic Solution Studies. *Int. J. Mass Spectrom. Ion Process.* **1998**, *174* (1−3), 219−230.

(4) Horowitz, Y.; Asscher, M. Low Energy Charged Particles Interacting with Amorphous Solid Water Layers. *J. Chem. Phys.* **2012**, *136* (13), No. 134701.

(5) Shin, S.; Kim, Y.; Moon, E.; Lee, D. H.; Kang, H.; Kang, H. Generation of Strong Electric Fields in an Ice Film Capacitor. *J. Chem. Phys.* **2013**, *139* (7), No. 074201.

(6) Bu, C.; Shi, J.; Raut, U.; Mitchell, E. H.; Baragiola, R. A. Effect of Microstructure on Spontaneous Polarization in Amorphous Solid Water Films. *J. Chem. Phys.* **2015**, *142* (13), No. 134702.

(7) Pilidi, A. N.; Gavra, I. K.; Tsekouras, A. A. Spontaneous Polarization of Cryo-Deposited Films for Five Normal Saturated Monohydroxy Alcohols, $C_nH_{2n+1}OH$, n = 1−5. *J. Phys. Chem. B* **2019**, *123* (40), 8505−8511.

(8) Sagi, R.; Akerman, M.; Ramakrishnan, S.; Asscher, M. Solid Ammonia Charging by Low-Energy Electrons. *J. Phys. Chem. C* **2021**, *125* (7), 3845−3858.

(9) Tourlakis, G. M.; Adamopoulos, S. A. T.; Gavra, I. K.; Milpanis, A. A.; Tsagri, L. F.; Pachygianni, A. S. G.; Chatzikokolis, S. S.; Tsekouras, A. A. Sign Flipping of Spontaneous Polarization in Vapour-Deposited Films of Small Polar Organic Molecules. *Phys. Chem. Chem. Phys.* **2021**, *23* (26), 14352−14362.

(10) Akerman, M.; Sagi, R.; Asscher, M. Charging Amorphous Solid Water Films by Ne^+ Ions Characterized by Contact Potential Difference Measurements. *J. Phys. Chem. C* **2020**, *124* (42), 23270−23279.

(11) Field, D.; Plekan, O.; Cassidy, A.; Balog, R.; Jones, N. C.; Dunger, J. Spontaneous Electric Fields in Solid Films: Spontelectrics. *Int. Rev. Phys. Chem.* **2013**, *32* (3), 345−392.

(12) Sagi, R.; Akerman, M.; Ramakrishnan, S.; Asscher, M. The Role of Thermal History on Spontaneous Polarization and Phase Transitions of Amorphous Solid Water Films Studied by Contact Potential Difference Measurements. *J. Chem. Phys.* **2020**, *153* (14), No. 144702.

(13) Sagi, R.; Akerman, M.; Ramakrishnan, S.; Asscher, M. Spontaneous Polarization of Thick Solid Ammonia Films. *J. Chem. Phys.* **2020**, *153* (12), No. 124707.

(14) Cassidy, A.; McCoustra, M. R. S.; Field, D. A Spontaneously Electrical State of Matter. *Acc. Chem. Res.* **2023**, *56* (14), 1909−1919.

(15) Stähler, J.; Meyer, M.; Bovensiepen, U.; Wolf, M. Solvation Dynamics of Surface-Trapped Electrons at NH_3 and D_2O Crystallites Adsorbed on Metals: From Femtosecond to Minute Timescales. *Chem. Sci.* **2011**, *2* (5), 907.

(16) Sagi, R.; Akerman, M.; Ramakrishnan, S.; Asscher, M. Temperature Effect on Transport, Charging, and Binding of Low-Energy Electrons Interacting with Amorphous Solid Water Films. *J. Phys. Chem. C* **2018**, *122* (18), 9985−9996.
(17) Park, Y.; Shin, S.; Kang, H. Recent Progress in the Manipulation of Molecules with DC Electric Fields. *Acc. Chem. Res.* **2021**, *54* (2), 323−331.
(18) Shaik, S.; Mandal, D.; Ramanan, R. Oriented Electric Fields as Future Smart Reagents in Chemistry. *Nat. Chem.* **2016**, *8* (12), 1091−1098.
(19) Arumainayagam, C. R.; Lee, H.-L.; Nelson, R. B.; Haines, D. R.; Gunawardane, R. P. Low-Energy Electron-Induced Reactions in Condensed Matter. *Surf. Sci. Rep.* **2010**, *65* (1), 1−44.
(20) Lu, Q.-B.; Sanche, L. Enhanced Dissociative Electron Attachment to CF_2Cl_2 by Transfer of Electrons in Precursors to the Solvated State in Water and Ammonia Ice. *Phys. Rev. B* **2001**, *63* (15), No. 153403.
(21) Boudaïffa, B.; Cloutier, P.; Hunting, D.; Huels, M. A.; Sanche, L. Resonant Formation of DNA Strand Breaks by Low-Energy (3 to 20 eV) Electrons. *Science* **2000**, *287* (5458), 1658.
(22) Zheng, Y.; Sanche, L. Effective and Absolute Cross Sections for Low-Energy (1−30 eV) Electron Interactions with Condensed Biomolecules. *Appl. Phys. Rev.* **2018**, *5* (2), No. 021302.
(23) Alizadeh, E.; Sanz, A. G.; García, G.; Sanche, L. Radiation Damage to DNA: The Indirect Effect of Low-Energy Electrons. *J. Phys. Chem. Lett.* **2013**, *4* (5), 820−825.
(24) Altwegg, K.; Balsiger, H.; Bar-Nun, A.; Berthelier, J.-J.; Bieler, A.; Bochsler, P.; Briois, C.; Calmonte, U.; Combi, M. R.; Cottin, H.; et al. Prebiotic Chemicals-Amino Acid and Phosphorus-in the Coma of Comet 67P/Churyumov-Gerasimenko. *Sci. Adv.* **2016**, *2* (5), No. e1600285.
(25) Öberg, K. I. Photochemistry and Astrochemistry: Photochemical Pathways to Interstellar Complex Organic Molecules. *Chem. Rev.* **2016**, *116* (17), 9631−9663.
(26) Kimmel, G. A.; Orlando, T. M.; Vézina, C.; Sanche, L. Low-energy Electron-stimulated Production of Molecular Hydrogen from Amorphous Water Ice. *J. Chem. Phys.* **1994**, *101* (4), 3282−3286.
(27) Ayotte, P.; Gamache, J.; Bass, A. D.; Fabrikant, I. I.; Sanche, L. Absolute Cross Sections for Dissociative Electron Attachment to Condensed CH_3Cl and CH_3Br: Effects of Potential Energy Curve Crossing and Capture Probability. *J. Chem. Phys.* **1997**, *106* (2), 749−760.
(28) Lias, S. G. Ionization Energy Evaluation. In *NIST Chemistry WebBook, NIST Standard Reference Database Number 69*; Linstrom, P. J., Mallard, W. G., Eds.; National Institute of Standards and Technology: Gaithersburg MD, p 20899.
(29) Schwentner, N.; Himpsel, F.-J.; Saile, V.; Skibowski, M.; Steinmann, W.; Koch, E. E. Photoemission from Rare-Gas Solids: Electron Energy Distributions from the Valence Bands. *Phys. Rev. Lett.* **1975**, *34*, 528−531, DOI: 10.1103/physrevlett.34.528.
(30) Redhead, P. A. Thermal Desorption of Gases. *Vacuum* **1962**, *12* (4), 203−211.
(31) Ferreira, A. G. M.; Lobo, L. Q. The Sublimation of Argon, Krypton, and Xenon. *J. Chem. Thermodyn.* **2008**, *40* (12), 1621−1626.
(32) Dowell, L. G.; Rinfret, A. P. Low-Temperature Forms of Ice as Studied by X-Ray Diffraction. *Nature* **1960**, *188* (4757), 1144−1148.
(33) Mayer, E.; Pletzer, R. Astrophysical Implications of Amorphous Ice- a Microporous Solid. *Nature* **1986**, *319* (6051), 298−301.
(34) Hashemi, S. R.; McCoustra, M. R. S.; Fraser, H. J.; Nyman, G. A Theoretical Study on Spontaneous Dipole Orientation in Ice Structures. *Phys. Chem. Chem. Phys.* **2022**, *24* (21), 12922−12925.
(35) Brown, D. E.; George, S. M.; Huang, C.; Wong, E. K. L.; Rider, K. B.; Smith, R. S.; Kay, B. D. H_2O Condensation Coefficient and Refractive Index for Vapor-Deposited Ice from Molecular Beam and Optical Interference Measurements. *J. Phys. Chem.* **1996**, *100* (12), 4988−4995.
(36) Bossa, J.-B.; Isokoski, K.; de Valois, M. S.; Linnartz, H. Thermal Collapse of Porous Interstellar Ice. *Astron. Astrophys.* **2012**, *545*, A82.
(37) Berland, B. S.; Brown, D. E.; Tolbert, M. A.; George, S. M. Refractive Index and Density of Vapor-Deposited Ice. *Geophys. Res. Lett.* **1995**, *22* (24), 3493−3496.
(38) Bar-Nun, A.; Dror, J.; Kochavi, E.; Laufer, D. Amorphous Water Ice and Its Ability to Trap Gases. *Phys. Rev. B* **1987**, *35* (5), 2427−2435.
(39) Lilach, Y.; Asscher, M. Compression and Caging of CD_3Cl by H_2O Layers on Ru(001). *J. Chem. Phys.* **2002**, *117* (14), 6730−6736.
(40) Livneh, T.; Romm, L.; Asscher, M. Cage Formation of N_2 under H_2O Overlayer on Ru(001). *Surf. Sci.* **1996**, *351* (1), 250−258.
(41) Smith, R. S.; Huang, C.; Wong, E. K. L.; Kay, B. D. The Molecular Volcano: Abrupt CCl_4 Desorption Driven by the Crystallization of Amorphous Solid Water. *Phys. Rev. Lett.* **1997**, *79* (5), 909−912.
(42) May, R. A.; Smith, R. S.; Kay, B. D. The Release of Trapped Gases from Amorphous Solid Water Films. II. "Bottom-up" Induced Desorption Pathways. *J. Chem. Phys.* **2013**, *138* (10), No. 104502.
(43) Akerman, M. S.; Sagi, R.; Asscher, M. Inverse Volcano: A New Molecule−Surface Interaction Phenomenon. *Phys. Rev. Lett.* **2023**, *130* (8), No. 086203.
(44) Ghosh, J.; Bhuin, R. G.; Vishwakarma, G.; Pradeep, T. Formation of Cubic Ice via Clathrate Hydrate, Prepared in Ultrahigh Vacuum under Cryogenic Conditions. *J. Phys. Chem. Lett.* **2020**, *11* (1), 26−32.
(45) Tsekouras, A. A.; Iedema, M. J.; Cowin, J. P. Amorphous Water-Ice Relaxations Measured with Soft-Landed Ions. *Phys. Rev. Lett.* **1998**, *80* (26), 5798−5801.

https://doi.org/10.1021/acs.jpcc.3c07591
J. Phys. Chem. C 2024, 128, 651−657